

A TEST OF STAR FORMATION LAWS IN DISK GALAXIES. II. DEPENDENCE ON DYNAMICAL PROPERTIES

CHUTIPONG SUWANNAJAK¹, JONATHAN C. TAN^{1,2}, ADAM K. LEROY³

¹Department of Astronomy, University of Florida, Gainesville, Florida 32611, USA

²Department of Physics, University of Florida, Gainesville, Florida 32611, USA

³National Radio Astronomy Observatory, 520 Edgemont Road, Charlottesville, Virginia 22903, USA

Accepted to the Astrophysical Journal

ABSTRACT

We use the observed radial profiles of the mass surface densities of total, Σ_g , and molecular, Σ_{H_2} , gas, rotation velocity and star formation rate (SFR) surface density, Σ_{sfr} , of the molecular-rich ($\Sigma_{\text{H}_2} \geq \Sigma_{\text{HI}}/2$) regions of 16 nearby disk galaxies to test several star formation laws: a “Kennicutt-Schmidt” law, $\Sigma_{\text{sfr}} = A_g \Sigma_{g,2}^{1.5}$; a “Constant Molecular” law, $\Sigma_{\text{sfr}} = A_{\text{H}_2} \Sigma_{\text{H}_2,2}$; the turbulence-regulated laws of Krumholz & McKee (KM05) and Krumholz, McKee & Tumlinson (KMT09), a “Gas- Ω ” law, $\Sigma_{\text{sfr}} = B_\Omega \Sigma_g \Omega$; and a shear-driven “GMC Collision” law, $\Sigma_{\text{sfr}} = B_{\text{CC}} \Sigma_g \Omega (1 - 0.7\beta)$, where $\beta \equiv d \ln v_{\text{circ}} / d \ln r$. If allowed one free normalization parameter for each galaxy, these laws predict the SFR with rms errors of factors of 1.4 to 1.8. If a single normalization parameter is used by each law for the entire galaxy sample, then rms errors range from factors of 1.5 to 2.1. Although the Constant Molecular law gives the smallest rms errors, the improvement over the KMT, Kennicutt-Schmidt and GMC Collision laws is not especially significant, particularly given the different observational inputs that the laws utilize and the scope of included physics, which ranges from empirical relations to detailed treatment of interstellar medium processes. We next search for systematic variation of star formation law parameters with local and global galactic dynamical properties of disk shear rate (related to β), rotation speed and presence of a bar. We demonstrate with high significance that higher shear rates enhance star formation efficiency per local orbital time. Such a trend is expected if GMC collisions play an important role in star formation, while an opposite trend would be expected if development of disk gravitational instabilities is the controlling physics.

Subject headings: stars: formation — galaxies: evolution

1. INTRODUCTION

Understanding the rate at which stars form from a given galactic gas inventory is a basic input for models of galaxy evolution. Global and kiloparsec-scale correlations between star formation activity, gas content and galactic dynamical properties have been observed (e.g., Kennicutt & Evans 2012). However, most star formation is known to occur in highly clustered $\sim 1 - 10$ pc-scale regions within giant molecular clouds (GMCs) and the physical processes linking these large and small scales, i.e., the “micro-physics” of galactic star formation laws, remain uncertain.

Tan (2010, hereafter Paper I), analyzed data from Leroy et al. (2008) for the molecular dominated regions of 12 nearby disk galaxies. The predictions of six star formation laws, described below, were tested against the observed radial profiles in the galaxies.

In this paper, after summarizing the star formation (SF) laws to be considered (§2) and adopting similar methods as Paper I (§3), we have extended this work by: (1) utilizing a modestly expanded sample of 16 galaxies, which are now explicitly selected to be relatively large disk galaxies with mean circular velocity $\geq 100 \text{ km s}^{-1}$ (11 galaxies overlap with the sample of Paper I); (2) also considering “molecular rich” regions where $\Sigma_{\text{HI}}/2 < \Sigma_{\text{H}_2} < \Sigma_{\text{HI}}$, in addition to the “molecular dominated” regions (the results of relative comparison of the different SF laws in these regions are presented in §4.1); (3) searching for correlations of SF law parameters with galactic dynamical properties (§4.2), i.e., galactic disk shear (rotation curve gradient), rotation speed, and presence of a bar. We conclude in §5.

2. OVERVIEW OF STAR FORMATION “LAWS” TO BE TESTED

Here we overview the various star formation “laws” that we will test in this paper. These vary in their nature from being simple empirical relations to being the predictions of more detailed models of physical processes in galactic interstellar media. There are also varying ranges of physical conditions over which these laws are expected to be valid. We note also that the measurement of star formation rates and gas masses, which are key ingredients in these laws suffer from significant systematic, potentially correlated, uncertainties (see, e.g., discussions in Leroy et al. 2008, 2013; Sandstrom et al. 2013).

Considering global disk-averages, Kennicutt (1998) presented an empirical relation, hereafter the Kennicutt-Schmidt law, between the disk plane surface density of star formation rate (SFR), Σ_{sfr} , and the total gas mass surface density:

$$\Sigma_{\text{sfr}} = A_g \Sigma_{g,2}^{\alpha_g}, \quad (1)$$

where $A_g = 0.158 \pm 0.044 M_\odot \text{ yr}^{-1} \text{ kpc}^{-2}$, $\Sigma_{g,2} = \Sigma_g / 100 M_\odot \text{ pc}^{-2}$, and $\alpha_g = 1.4 \pm 0.15$. The dynamic range of this relation covers from the molecular-rich regions of normal galaxies to the molecular-dominated regions in galactic centers and in

starburst galaxies. Theoretical and numerical models that relate the SFR to the growth rate of large scale gravitational instabilities in a disk predict $\alpha_g \simeq 1.5$ (e.g. Larson 1988; Elmegreen 1994, 2002; Wang & Silk 1994; Li, Mac Low, & Klessen 2006), as long as the gas scale height does not vary much from galaxy to galaxy or, for a local form of the relation, within the galaxy.

Alternatively, based on a study of 12 nearby disk galaxies resolved at ~ 1 kpc resolution, Leroy et al. (2008) (see also Bigiel et al. 2008) concluded that

$$\Sigma_{\text{sfr}} = A_{\text{H2}} \Sigma_{\text{H2},2}, \quad (2)$$

where $A_{\text{H2}} = (5.25 \pm 2.5) \times 10^{-2} M_{\odot} \text{yr}^{-1} \text{kpc}^{-2}$ and $\Sigma_{\text{H2},2} = \Sigma_{\text{H2}}/100 M_{\odot} \text{pc}^{-2}$. The values of Σ_{H2} covered a range from $\sim 4 - 100 M_{\odot} \text{pc}^{-2}$ and were estimated assuming a constant “X” conversion factor of CO line emission to H_2 column density. Leroy et al. (2013) have shown that, from a similar study of 30 nearby disk galaxies, $A_{\text{H2}} = 4.5 \times 10^{-2} M_{\odot} \text{yr}^{-1} \text{kpc}^{-2}$ or $\tau_{\text{dep}}^{\text{H2}} = \Sigma_{\text{H2}}/\Sigma_{\text{sfr}} = A_{\text{H2}}^{-1} = 2.2 \text{ Gyr}$ with ≈ 0.3 dex scatter. This star formation relation will be referred to as the Constant Molecular law.

The turbulence-regulated star formation model of Krumholz & McKee (2005) (hereafter the KM05 law) predicts galactic star formation rates by assuming GMCs are virialized and that their surfaces are in pressure equilibrium with the large scale interstellar medium (ISM) pressure of a Toomre (1964) $Q \simeq 1.5$ disk. They predict

$$\Sigma_{\text{sfr}} = A_{\text{KM}} f_{\text{GMC}} \phi_{\bar{P},6}^{0.34} Q_{1.5}^{-1.32} \Omega_0^{1.32} \Sigma_{g,2}^{0.68}, \quad (3)$$

where $A_{\text{KM}} = 9.5 M_{\odot} \text{yr}^{-1} \text{kpc}^{-2}$, f_{GMC} is the mass fraction of gas in GMCs, $\phi_{\bar{P},6}$ is the ratio of the mean pressure in a GMC to the surface pressure here normalized to a fiducial value of 6 but estimated to vary as $\phi_{\bar{P}} = 10 - 8 f_{\text{GMC}}$, $Q_{1.5} = Q/1.5$, and Ω_0 is Ω , the orbital angular frequency, in units of Myr^{-1} . We assume that $f_{\text{GMC}} = \Sigma_{\text{H2}}/\Sigma_g$ based on resolved studies of GMC populations and molecular gas content in the Milky Way and nearby galaxies (Solomon et al. 1987; Blitz et al. 2007).

Krumholz, McKee & Tumlinson (2009) (hereafter the KMT09 law) presented a two component turbulence-regulated star formation law

$$\Sigma_{\text{sfr}} = A_{\text{KMT}} f_{\text{GMC}} \Sigma_{g,2} \times \begin{cases} (\Sigma_g/85 M_{\odot} \text{pc}^{-2})^{-0.33}, & \Sigma_g < 85 M_{\odot} \text{pc}^{-2} \\ (\Sigma_g/85 M_{\odot} \text{pc}^{-2})^{0.33}, & \Sigma_g > 85 M_{\odot} \text{pc}^{-2} \end{cases} \quad (4)$$

where $A_{\text{KMT}} = 3.85 \times 10^{-2} M_{\odot} \text{yr}^{-1} \text{kpc}^{-2}$. GMCs are assumed to be in pressure equilibrium with the ISM only in the high Σ_g regime. In the low regime, GMCs are assumed to have constant internal pressures set by H II region feedback (Matzner 2002). Krumholz et al. (2012) presented a test of this turbulence regulated star formation law against observations of star formation from scales of individual GMCs to entire galaxies.

K1998 also showed that his galaxy and circumnuclear starburst data could be fit by a star formation law with direct dependence on galactic orbital dynamics:

$$\Sigma_{\text{sfr}} = B_{\Omega} \Sigma_g \Omega, \quad (5)$$

hereafter the Gas- Ω law, where $B_{\Omega} = 0.017$ and Ω is evaluated at the outer radius that is used to perform the disk averages. This law has also been studied in samples of galaxies and starbursts extending to higher redshifts by, for example, Genzel et al. (2010), Daddi et al. (2010) and García-Burillo et al. (2012). It implies that a fixed fraction, about 10%, of the gas is turned into stars every outer orbital timescale of the star-forming disk and motivates theoretical models that relate star formation activity to the dynamics of galactic disks.

In order to link global galactic dynamics with the scales of star-forming regions in GMCs, Tan (2000) proposed a model of star formation triggered by GMC collisions in a shearing disk, which reproduces eq. (5) in the limit of a flat rotation curve since the collision time is estimated to be a short and approximately constant fraction, $\sim 20\%$, of the orbital time, t_{orbit} . This behavior of the GMC collision time was confirmed in the numerical simulations of Tasker & Tan (2009). The GMC Collision model assumes a Toomre Q parameter of order unity in the star-forming part of the disk, a significant fraction (e.g. $\gtrsim 1/3$) of total gas in gravitationally bound clouds, and a velocity dispersion of these clouds set by gravitational scattering (Gammie et al. 1991). Then, the predicted SFR is

$$\Sigma_{\text{sfr}} = B_{\text{CC}} Q^{-1} \Sigma_g \Omega (1 - 0.7\beta), \quad (\beta \ll 1) \quad (6)$$

where $\beta \equiv d \ln v_{\text{circ}}/d \ln r$ and v_{circ} is the circular velocity at a particular galactocentric radius r . Note that $\beta = 0$ for a flat rotation curve. There is a prediction of reduced star formation efficiencies per orbit compared to eq. (5) in regions with reduced shear, i.e. typically the inner parts of disk galaxies.

The above six laws are not the only ones that have been proposed. For example, Ostriker, McKee, and Leroy (2010) suggested a self-regulated star formation model for disk galaxies (though mostly focussed on the more H I-rich outer regions compared to our present study), $\Sigma_{\text{sfr}} \propto \Sigma_g \sqrt{\rho_{\text{sd}}}$, where ρ_{sd} is the midplane volume density of stars and dark matter. However, this volume density is difficult to evaluate empirically.

Paper I showed that the KMT2009 turbulence-regulated, constant molecular, and GMC collision models can produce the observed SFRs with rms error of about a factor of 1.5, where each galaxy is allowed one free parameter. The other models do moderately worse with larger rms error of factor of 1.8 and 2.0 for Gas- Ω and KM2005 turbulence-regulated models, respectively.

3. METHODOLOGY

We utilize data presented by Leroy et al. (2013), providing Σ_{H_2} , Σ_{HI} , Σ_{sfr} , v_{circ} , and β of 30 nearby disk galaxies (see also Schruba et al. 2011). We refer the reader to Leroy et al. (2013) for the methods used to estimate these quantities. We note that v_{circ} and β are based on simple parameterized fits to tilted ring modeling (de Blok et al. 2008) based on HI (Walter et al. 2008) and CO data. The fits wash out $\sim\text{kpc}$ -scale variations in the rotation curve.

We focus only on the galaxies which have some regions where molecular gas dominates over atomic, $\Sigma_{\text{H}_2} \geq \Sigma_{\text{HI}}$. There are 21 galaxies that fulfill this criterion, including the 12 galaxies analyzed in Paper I. Our focus is on “large” disk galaxies, so we restrict further analysis to systems with $\bar{v}_{\text{circ}} > 100 \text{ km s}^{-1}$ in the molecular dominated region. One motivation for this is to exclude dwarf galaxies, which may have larger systematic differences in properties such as metallicity that can affect estimates of molecular gas mass. This leaves 16 galaxies in our sample: 5 new galaxies compared to Paper I, and 1 galaxy from Paper I (NGC 3198) now excluded.

Table 1 lists the basic properties of our galaxy sample. The morphological types and distances are assessed from the NASA/IPAC Extragalactic Database (NED). Galactic radii (r_{B25}) are adopted from Leroy et al. (2013). Finally, the last two columns show average circular velocity from the rotation curve, \bar{v} , and average logarithmic derivative of the rotation curve, $\bar{\beta}$. Typically, galaxies in our sample have $\bar{\beta} \lesssim 0.4$ and $\bar{v} \gtrsim 150 \text{ km s}^{-1}$ except NGC 3184 that has $\bar{\beta} \sim 0.6$ and $\bar{v}_{\text{circ}} \sim 120 \text{ km s}^{-1}$.

Following the method of Paper I, we fit the observed data of molecular dominated regions of the sample galaxies with the six star formation laws described in §1 to derive the best-fit values of A_{g} , A_{H_2} , A_{KM} , A_{KMT} , B_{Ω} , and B_{CC} , from a Kennicutt-Schmidt law (Eq. 1), using $\alpha_{\text{g}} = 1.5$, the Constant Molecular law (Eq. 2), the KM05 turbulence regulated law (Eq. 3), calculating the orbital angular frequency, Ω , from the given v_{circ}/r and setting the value of $Q = 1$, a KMT09 turbulence regulated law (Eq. 4), the Gas- Ω law (Eq. 5), and the GMC Collision law (Eq. 6), setting $Q = 1.5$. The outer radius, r_{out} , of the sample galaxies is determined by the radius where molecular gas dominates over atomic gas, $\Sigma_{\text{H}_2} \geq \Sigma_{\text{HI}}$. For NGC 2814, molecular gas is not dominant over atomic gas in the central region but it becomes so at about 2 kpc.

The best-fit star formation law parameters are constrained by comparing $\Sigma_{\text{sfr, theory}}$ from these six star formation laws with the observed $\Sigma_{\text{sfr, obs}}$. For each galaxy we derive χ , where $\chi^2 \equiv (N_{\text{ann}} - N_{\text{fit}})^{-1} \sum (\log_{10} R_{\text{sfr}})^2$, N_{ann} is the number of resolved annuli in the galaxy, $R_{\text{sfr}} = \Sigma_{\text{sfr, theory}}/\Sigma_{\text{sfr, obs}}$, and $N_{\text{fit}} = 1$ (note, each star formation law has one free parameter). We also carry out this analysis for the entire sample and for sub-samples in two ways. First each galaxy is allowed one free parameter so that N_{fit} equals the number of galaxies in the sample (i.e., 16) or sub-sample. Second, we fit for a single star formation law for the sample or sub-sample with one global free parameter ($N_{\text{fit}} = 1$). The values of χ and the rms dispersions of the data about the best fits are considered.

We repeat the above analysis for “molecular rich” regions with $\Sigma_{\text{HI}}/2 < \Sigma_{\text{H}_2} < \Sigma_{\text{HI}}$, which typically applies to an extended annulus in the galaxy out to a radius r_{ext} . Only galaxies with $N_{\text{ann}} \geq 3$ in the molecular rich region are analyzed, i.e. 14 galaxies. Finally, we also carry out the analysis on the combined molecular dominated and rich regions for all the galaxies.

With 16 galaxies, we are now in a position to also examine trends of star formation law parameters with galaxy properties, both by defining and comparing sub-samples and looking for correlations with continuous variables.

TABLE 1
BASIC PROPERTIES OF SAMPLE GALAXIES

Galaxy NGC:	Messier Index	Morphological Type	d (Mpc)	r_{B25} (kpc)	r_{out} (kpc)	r_{ext} (kpc)	\bar{v}_{circ} (km s^{-1})	$\bar{\beta}$
0628*	M74	SA(s)c	9.7	10.4	4.5	5.6	181	0.272
2841*	-	SA(r)b	15.4	14.2	7.8	10.0	300	0.022
2903	-	SAB(rs)bc	9.3	15.2	5.2	5.7	145	0.410
3184*	-	SAB(rs)cd	12.6	-	5.4	6.8	119	0.608
3351*	M95	SB(r)b	9.9	10.6	5.6	7.5	171	0.209
3521*	-	SAB(rs)bc	11.5	12.9	5.9	6.9	175	0.367
3627*	M66	SAB(s)b	10.1	13.8	8.1	8.4	164	0.237
4254	M99	SA(s)c	15.6	14.6	9.1	12.3	150	0.337
4321	M100	SAB(s)bc	15.8	12.5	8.8	11.0	176	0.320
4579	M58	SAB(rs)b	19.4	15.0	10.7	11.4	209	0.320
4736*	M94	(R)SA(r)ab	4.9	5.3	2.0	4.2	145	0.118
5055*	M63	SA(rs)bc	8.2	17.3	8.4	10.0	177	0.132
5194*	M51	SA(s)bc pec	8.1	9.0	6.9	7.9	195	0.181
5457	M101	SAB(rs)cd	7.0	25.8	6.9	9.0	182	0.270
6946*	-	SAB(rs)cd	5.5	9.8	6.0	7.5	145	0.351
7331*	-	SA(s)b	14.5	19.5	7.2	9.0	202	0.284

*Analyzed in Paper I

4. RESULTS

4.1. *Test of Star Formation Laws*

First, we examine how well the star formation laws described in §2 do in predicting the SFR as a function of galactocentric radius, given their required inputs. Note that these input requirements differ: e.g. the Constant Molecular law only needs the surface density of molecular gas, while some of the other laws require multiple inputs, each of which has inherent observational uncertainties. Thus, while the relative accuracy with which the laws can predict SFRs is still interesting (e.g., if one is concerned with how accurate the use of given law will be in a model of galaxy evolution), this relative ordering may not necessarily distinguish between which physical mechanism(s) is responsible for setting SFRs. In addition, there

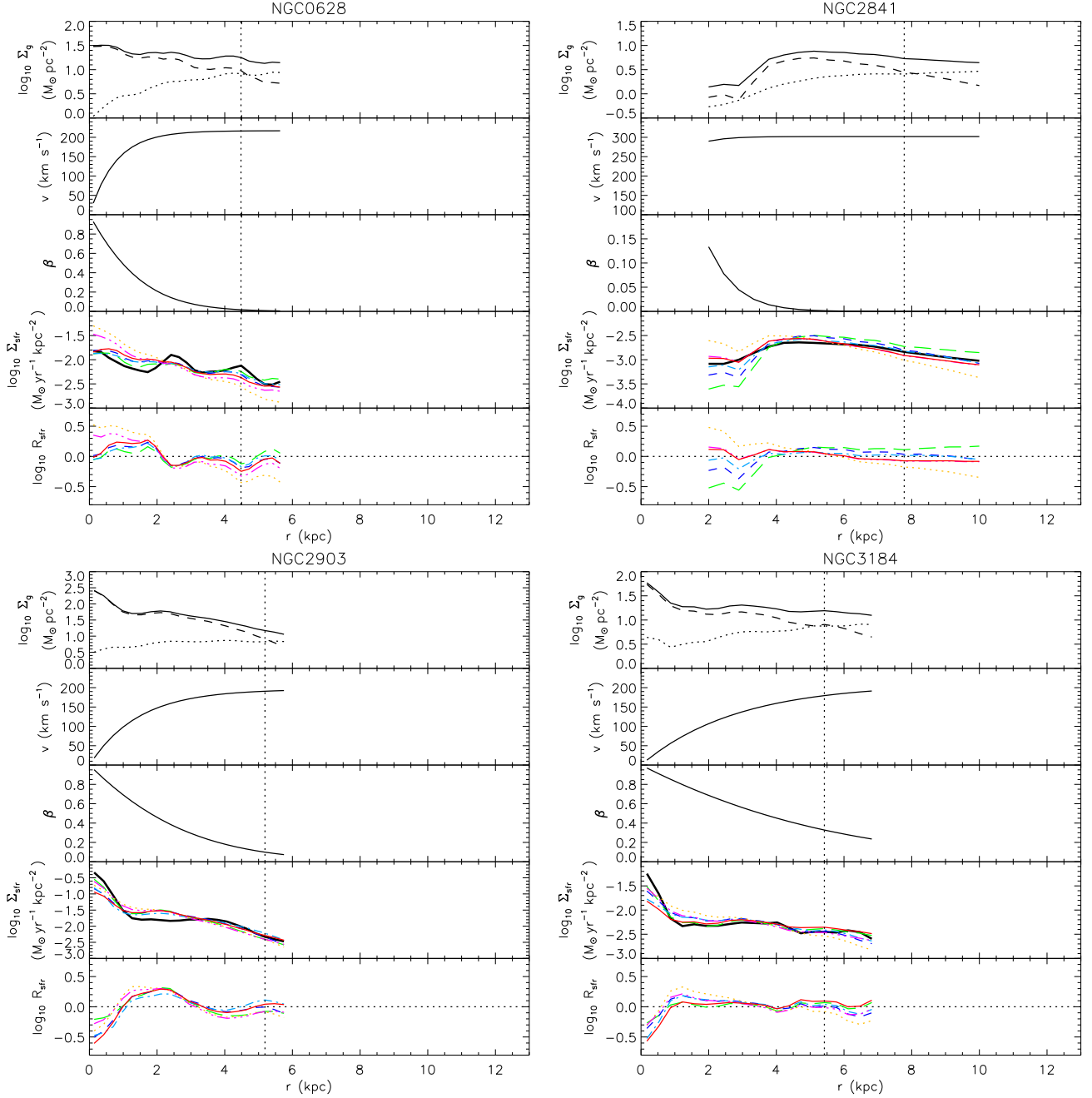


FIG. 1.— Radial distribution of properties of NGC 0628, NGC 2841, NGC 2903, and NGC 3184, as indicated, for the regions where $\Sigma_{\text{H}_2} \geq \Sigma_{\text{HI}}/2$. In each 5-panel figure, the top panel shows radial profiles of surface density of molecular hydrogen, Σ_{H_2} , (dashed), atomic hydrogen, Σ_{HI} , (dotted) and total gas (solid). The dotted vertical line indicates r_{out} , where Σ_{H_2} becomes less than Σ_{HI} . The second and third panels show the rotation velocity curve, v , and its logarithmic derivative, β , respectively. The fourth panel shows the predicted SFR surface density compared with the observed data (thick-dotted). Each star formation law is represented by: Kennicutt-Schmidt (Eq. 1; green long-dashed), Constant Molecular (Eq. 2; blue dashed), KM05 (Eq. 3; orange dotted), KMT09 (Eq. 4; cyan dot-dashed), Gas- Ω (Eq. 5; magenta dot-dot-dashed), and GMC Collision law (Eq. 6; red solid). Finally, the fifth panel shows $\log_{10} R_{\text{sfr}}$, i.e., \log_{10} of the ratio of the predicted SFR surface densities to the observed surface densities.

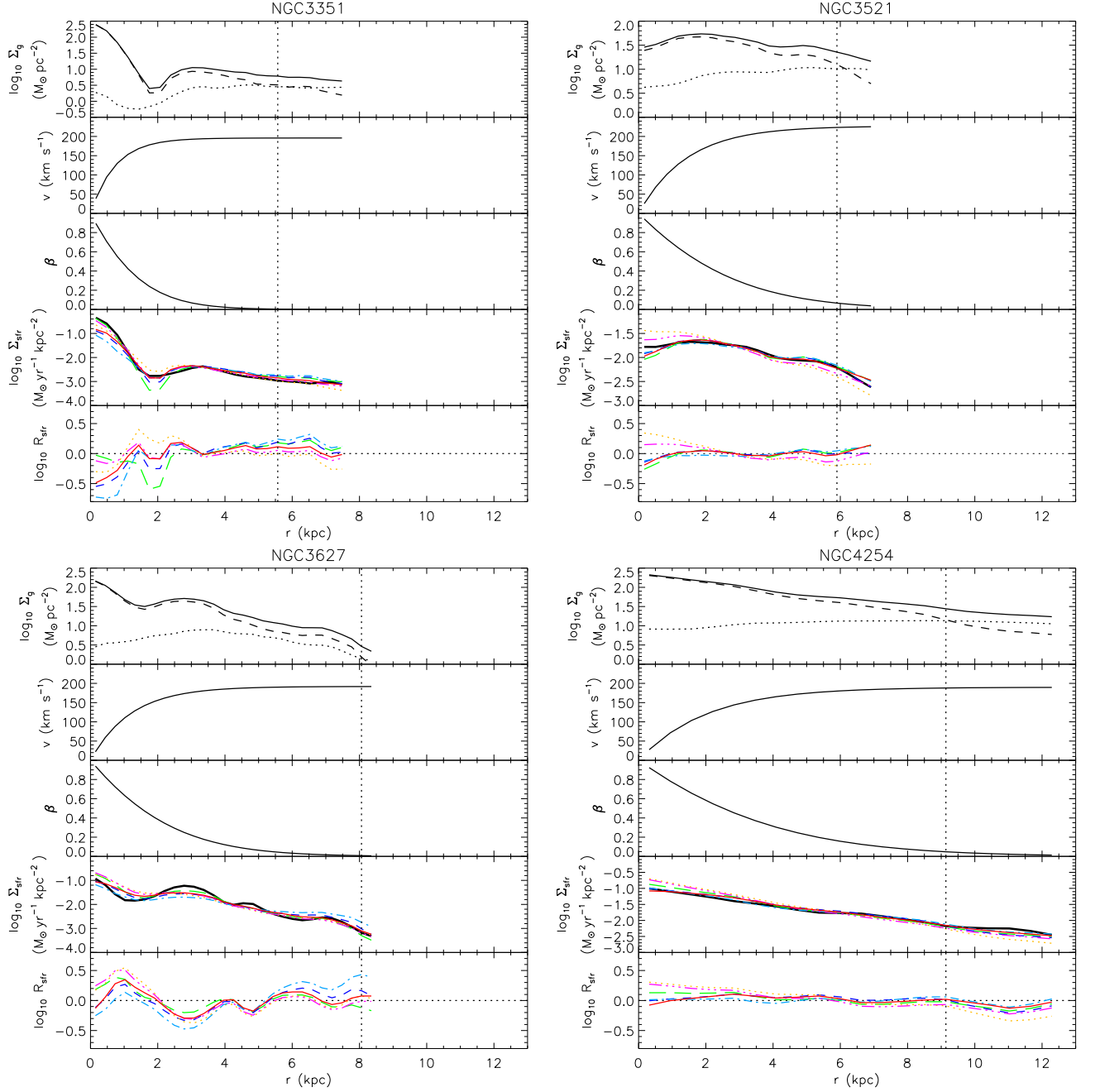


FIG. 2.— Radial distribution of properties of NGC 3351, NGC 3521, NGC 3627, and NGC 4254, with labeling as in Figure 1.

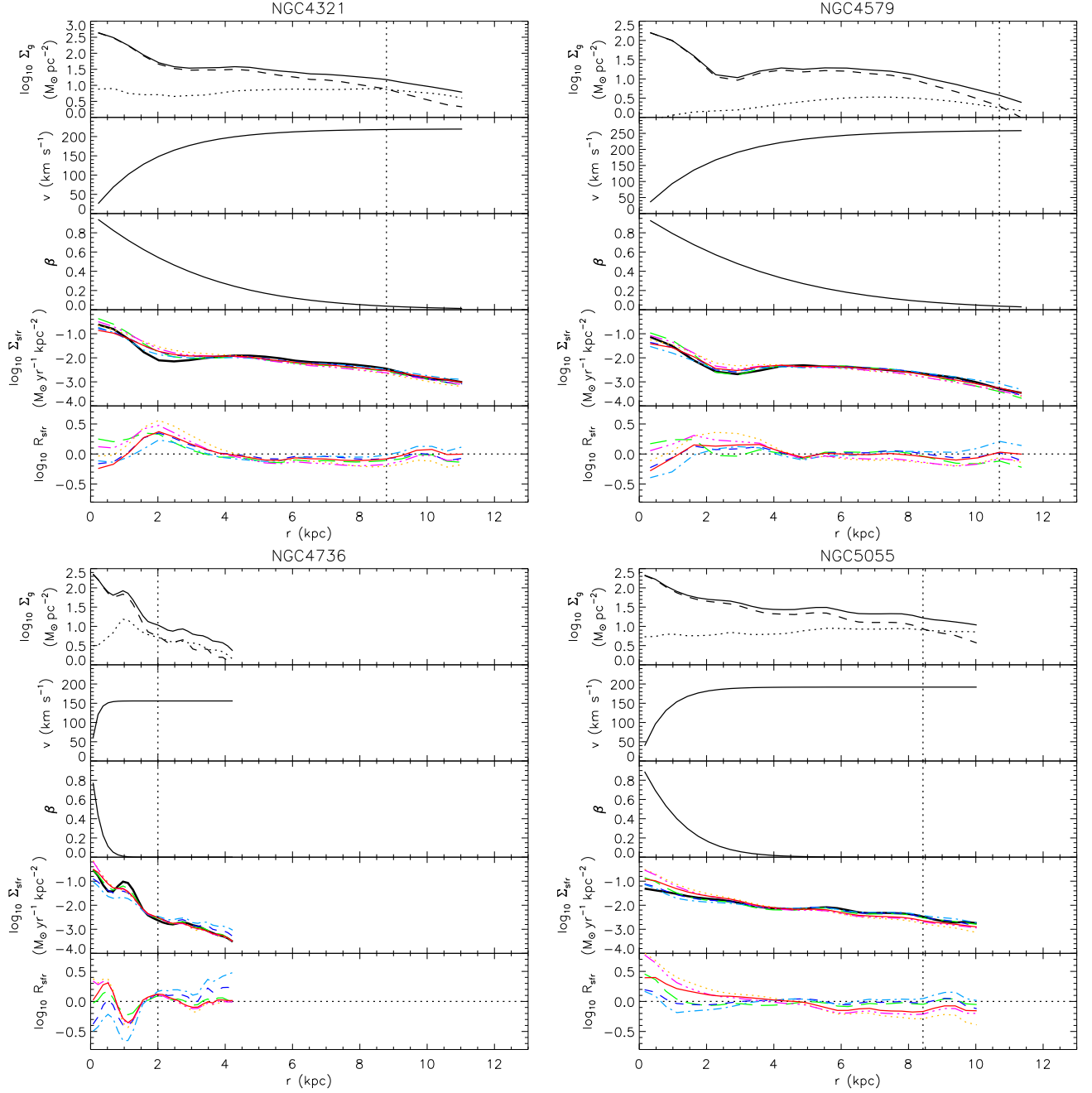


FIG. 3.— Radial distribution of properties of NGC 4321, NGC 4579, NGC 4736, and NGC 5055, with labeling as in Figure 1.

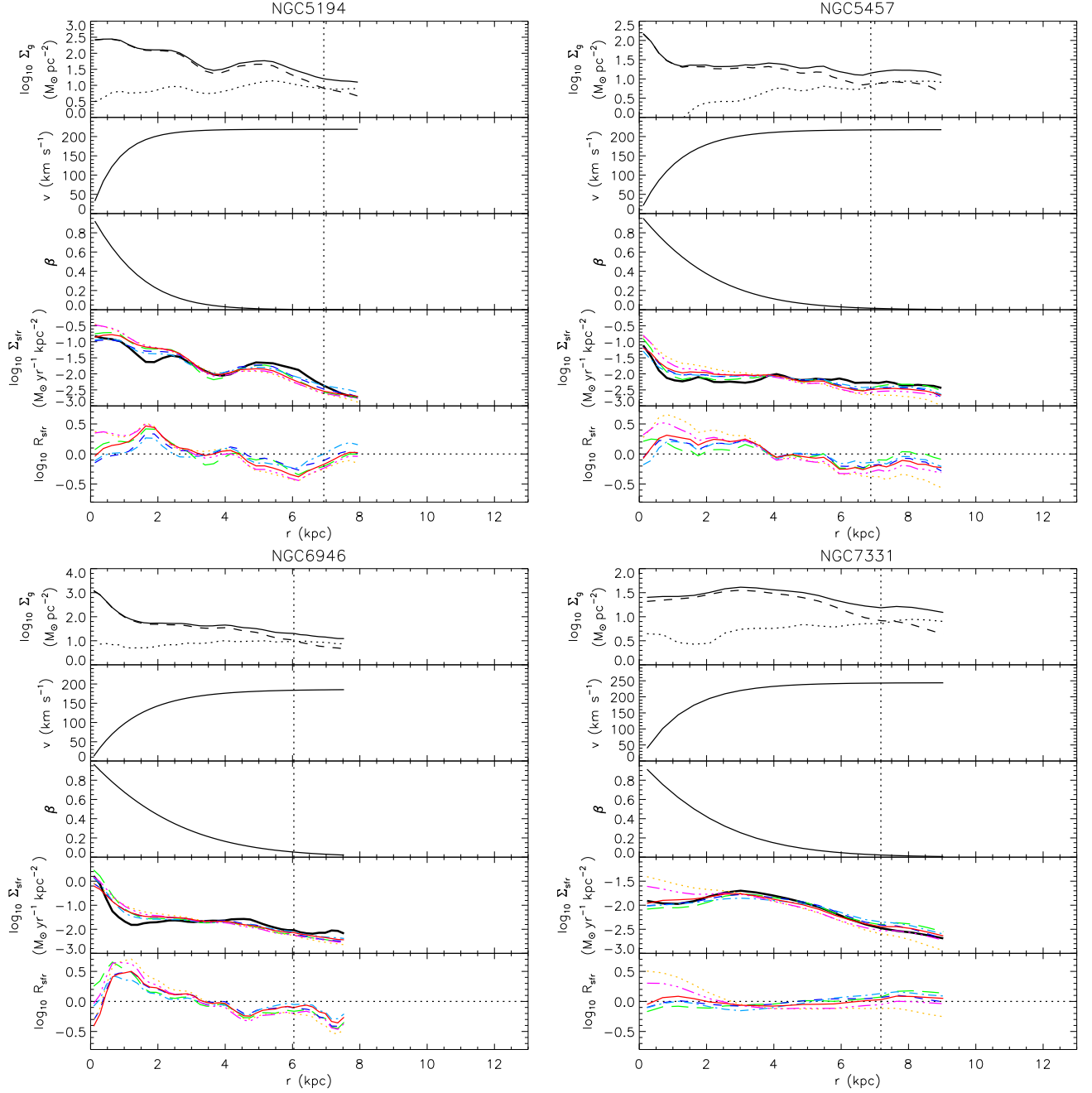


FIG. 4.— Radial distribution of properties of NGC 5194, NGC 5457, NGC 6946, and NGC 7331, with labeling as in Figure 1.

are different levels of physics built into these laws. The Constant Molecular law uses an input that is relatively close to star formation, namely the amount of molecular gas, without trying to predict why certain regions have a given molecular content. Other laws start with more basic global properties of the gas in the galaxy, such as its total gas content.

Figures 1 - 4 show the radial distribution of properties of the sample galaxies. The top panel shows observed profiles of molecular, atomic, and total gas mass surface density. The second and third panels show v_{circ} and β , respectively. The observed and predicted Σ_{sfr} are shown in the fourth panel. Finally, the last panel shows $\log_{10} R_{\text{sfr}}$. The vertical dotted line in each plot shows the position of r_{out} , where atomic gas becomes dominant over molecular gas.

Table 2 shows the best-fit parameters of the star formation laws as fit to the 16 sample galaxies, together with their goodness of fit parameters, χ . Results are shown separately for the molecular dominated regions, the molecular rich regions with $\Sigma_{\text{HI}}/2 < \Sigma_{\text{H}_2} < \Sigma_{\text{HI}}$ and the combined regions. For molecular dominated regions, when each galaxy is allowed one free parameter, the Constant Molecular law is the most accurate model, followed by the KMT09 law, the Kennicutt-Schmidt law, the GMC Collision law, the Gas- Ω law, and the KM05 law. But the first four have similar values of χ : the dispersion in the residuals of the GMC Collision law is a factor of 1.50, while that of the Constant Molecular law is 1.43. Even the worst-fitting relation, i.e. the KM05 law has a dispersion of only 1.82. The Constant Molecular law is still the best-fitting model when only one free parameter is allowed for the whole sample (with rms error of factor of 1.52), followed by the KMT09 law, the GMC collision law (rms error factor of 1.67), the Kennicutt-Schmidt law, the Gas- Ω law, and the KM05 law (rms error factor of 2.05).

For the extended molecular rich regions with $\Sigma_{\text{HI}}/2 < \Sigma_{\text{H}_2} < \Sigma_{\text{HI}}$, all the star formation laws still work reasonably well. When each galaxy with $N_{\text{ann}} \geq 3$ in such regions (note, NGC 3627 and NGC 4579 have $N_{\text{ann}} = 1$, so the analysis is not performed on them individually) has one free parameter, the ordering of the laws from best to worst is GMC Collision, Gas- Ω , Kennicutt-Schmidt, Constant Molecular, KM05, KMT09. However, again, the differences are relatively minor and a different ordering results when allowing only a single global free parameter (see Table 2).

Finally, the same analysis is repeated for the combined molecular dominated and rich regions (Table 2). The Constant Molecular law gives the best fit with rms error of a factor of 1.4 for the case of one free parameter per galaxy and 1.5 for the case of one global free parameter followed by the Kennicutt-Schmidt law, GMC Collision law, KMT09 law, Gas- Ω law, and KM05 law, which have rms error of factor of 1.8.

We summarize the rms dispersion of the fitted star formation law residuals, $\log_{10} R_{\text{sfr}}$, in Table 3. We attribute the smaller dispersion in the molecular rich regions to these being relatively narrow annular parts of galaxies that do not span a wide range of galactic properties, such as gas mass surface densities and orbital velocities. As described above, the differences between the different star formation laws are relatively modest. For molecular dominated or entire regions, there is a range from about a factor of 1.4 to 1.8 dispersion when allowing each galaxy one free parameter to normalize the star formation law, rising to 1.5 to 2.1 when a single global parameter is fit to the sample.

In Table 3 we also show the effect of excluding the central $r < 1$ kpc regions of the galaxies on the rms dispersions: these results are shown in parentheses. These central regions have poorly resolved rotation curves and have more uncertain molecular gas masses (Sandstrom et al. 2013; see also Bell et al. 2007; Israel et al. 2009). Excluding these regions always leads to a reduction in $\log_{10} R_{\text{sfr}}$, typically by $\sim 10 - 20\%$, and can result in occasional changes of the relative ordering of the different star formation laws. However, generally the Constant Molecular, Kennicutt-Schmidt, KMT09 and GMC Collision laws are seen to give quite similar rms values that are smaller than those of the KM05 and Gas- Ω laws. So we conclude that the results of the main analysis are not being adversely affected by the central kpc regions.

As described at the start of this section, the relative values of the dispersion between the different laws can result not only from the intrinsic merit of the physical model, but also because of the varying types of inputs and their associated observational uncertainties. The KMT09 law is an extension of the KM05 model, and it is seen to give improved fits to the data, i.e., with smaller dispersions. Likewise, the GMC Collision model can be regarded as a modification and extension of the dynamical Gas- Ω model: it uses the same inputs plus an additional one, the gradient of the rotation curve. This generally leads to a modest reduction of the dispersions of the data sets that include the molecular dominated regions where the largest rotation curve gradients are present (see also §4.2.1). The more empirical Kennicutt-Schmidt and Constant Molecular laws also provide good fits to the data, with the latter giving the (modestly) best fit for the molecular dominated and entire regions. However, this may reflect its more limited physical scope of starting with the observed amount of molecular gas as its input, rather than trying to connect star formation activity to more fundamental galactic properties.

4.2. Dependence of Star Formation Law Parameters on Galactic Dynamical Properties

We test the dependence of the derived star formation law parameters with three basic galactic dynamical properties: (1) Galactic Disk Shear, as measured by the gradient of the rotation curve; (2) Rotation Speed; (3) Presence of a Bar.

4.2.1. Galactic Disk Shear

We first divide the galaxy sample into “Low $\bar{\beta}$ ” and “High $\bar{\beta}$ ” sub-samples using a boundary of $\bar{\beta} = 0.3$. There are 9 Low $\bar{\beta}$ galaxies and 7 High $\bar{\beta}$ galaxies. We repeat the analysis of §4.1 for these two sub-samples and the results are shown in Table 4.

We carry out a two-sample Kolmogorov-Smirnov (KS) test to see if the distribution of derived star formation law parameters of the individual galaxies in each sub-sample, e.g., A_g , A_{H_2} , etc., are consistent with being drawn from the same parent distribution. The probabilities that they do come from the same distribution are also shown in Table 4. In

TABLE 2
STAR FORMATION LAW PARAMETERS

Galaxy NGC:	r_{out} (kpc)	N_{ann}	A_g^a (10^{-2})	χ_g (10^{-2})	$A_{\text{H}_2^a}$ (10^{-2})	χ_{H_2} (10^{-2})	A_{KM}^a (10^{-2})	χ_{KM} (10^{-2})	A_{KMT}^a (10^{-2})	χ_{KMT} (10^{-2})	B_Ω (10^{-3})	χ_Ω (10^{-2})	B_{CC} (10^{-3})	χ_{CC} (10^{-2})
Molecular Dominated regions														
0628	4.5	20	7.75	9.55	4.90	12.6	0.737	32.6	3.13	11.6	3.63	24.4	4.65	15.9
2841	7.8	14	17.1	27.2	5.66	16.0	0.786	19.7	2.14	7.39	5.33	7.65	5.42	6.99
2903	5.2	19	6.67	17.3	5.56	21.6	1.92	22.5	4.24	20.2	6.85	20.1	9.99	23.9
3184	5.4	16	6.81	9.11	4.28	13.1	1.56	16.7	2.66	17.3	6.21	12.4	11.2	17.9
3351	5.6	18	12.2	21.8	5.75	24.3	1.02	19.0	2.85	32.5	5.52	10.0	6.67	19.3
3521	5.9	18	6.13	8.54	4.90	4.81	1.36	17.7	3.71	4.93	5.22	11.0	7.31	5.69
3627	8.1	28	10.0	15.7	6.35	17.4	2.29	24.1	3.97	26.1	9.12	22.4	11.3	16.2
4254	9.1	15	4.00	7.41	4.38	3.37	3.38	13.8	3.62	3.13	8.64	13.2	11.7	4.95
4321	8.8	20	4.46	17.5	3.75	14.2	1.82	24.0	2.63	10.1	5.90	21.9	7.90	16.3
4579	10.7	17	5.27	12.0	2.72	8.57	1.06	18.6	1.55	14.7	4.60	15.7	6.16	11.1
4736	2.0	14	8.54	12.3	7.83	18.9	0.690	28.0	5.96	26.8	3.22	24.8	3.58	20.8
5055	8.4	27	4.46	12.8	3.65	5.82	1.45	29.8	2.65	8.36	4.99	26.2	5.63	16.9
5194	6.9	28	4.10	21.2	4.15	14.9	1.46	29.7	3.22	12.8	4.70	29.0	5.53	22.7
5457	6.9	30	6.67	13.8	4.06	15.0	1.13	33.1	2.62	13.3	4.91	27.3	6.27	18.8
6946	6.0	33	5.96	27.0	5.74	21.9	2.49	32.3	4.31	17.9	7.81	30.7	10.8	23.6
7331	7.2	16	7.18	6.48	4.82	5.10	1.31	23.5	3.33	8.86	5.50	15.5	7.12	5.11
$N_{\text{fit}}=16$		333		16.9		15.4		26.1		16.8		22.4		17.5
$N_{\text{fit}}=1$		333	6.55	22.9	4.74	18.2	1.45	31.2	3.17	20.5	5.66	24.8	7.28	22.4
Molecular Rich regions														
0628	5.6	5	7.04	8.67	6.35	5.32	2.10	5.15	3.52	5.75	6.18	7.13	6.22	7.20
2841	10.0	5	10.7	1.53	5.68	3.69	1.80	6.09	2.20	2.78	6.87	0.508	6.87	0.508
2903	5.7	2	8.43	2.21	6.79	4.44	2.82	4.01	3.59	2.92	8.45	1.32	8.95	1.05
3184	6.8	4	6.50	5.15	5.72	6.56	2.93	7.15	3.13	6.03	7.87	5.16	9.69	5.26
3351	7.5	6	7.93	6.30	3.90	10.1	1.50	11.5	1.53	8.59	5.90	7.01	5.91	6.99
3521	6.9	3	4.70	3.85	4.83	0.46	2.20	0.37	2.84	1.98	5.55	5.05	5.73	5.32
3627	8.4	1	15.0	-	5.24	-	2.10	-	1.56	-	9.43	-	9.47	-
4254	12.3	5	5.64	4.68	6.63	5.51	7.79	6.36	4.11	5.33	14.3	4.54	14.5	4.47
4321	11.0	5	5.50	5.93	4.28	4.99	2.86	4.62	2.02	4.42	7.35	4.59	7.46	4.59
4579	11.4	1	9.03	-	3.55	-	1.49	-	1.10	-	6.08	-	6.21	-
4736	4.2	15	7.92	4.17	4.13	7.73	0.811	7.61	1.68	12.4	3.64	6.01	3.64	6.01
5055	10.0	5	4.48	4.39	3.82	7.65	3.16	7.71	2.05	6.18	7.68	3.97	7.68	3.97
5194	7.9	4	4.68	6.47	4.03	3.91	2.15	3.43	2.20	4.54	5.83	6.04	5.84	6.05
5457	9.0	9	7.41	5.42	6.47	6.86	3.98	7.17	3.70	5.63	10.5	4.05	10.6	4.04
6946	7.5	8	13.2	12.1	12.2	12.0	7.27	13.0	6.80	10.1	18.3	11.8	18.8	11.5
7331	9.0	4	4.52	1.65	4.17	4.89	2.23	6.15	2.33	3.08	5.75	1.75	5.80	1.63
$N_{\text{fit}}=14$		80		6.24		7.40		7.90		8.00		6.20		6.16
$N_{\text{fit}}=1$		82	7.12	14.9	5.37	16.3	2.41	31.5	2.67	20.7	7.25	21.9	7.38	22.3
Combined Regions														
0628	5.6	25	7.60	9.36	5.16	12.3	0.908	34.5	3.20	10.8	4.04	23.9	4.93	15.4
2841	10.0	19	15.1	24.9	5.67	13.7	0.977	23.6	2.15	6.44	5.70	8.20	5.77	7.56
2903	5.7	21	6.82	16.7	5.66	20.7	1.99	22.0	4.17	19.3	6.99	19.2	9.89	22.7
3184	6.8	20	6.75	8.39	4.54	13.0	1.77	18.8	2.75	15.8	6.51	12.0	10.9	16.3
3351	7.5	24	10.9	20.7	5.22	22.7	1.12	18.8	2.44	30.7	5.62	9.31	6.47	17.1
3521	6.9	21	5.90	8.98	4.89	4.44	1.46	17.9	3.57	6.18	5.27	10.3	7.06	6.69
3627	8.4	29	10.2	15.8	6.31	17.1	2.28	23.7	3.85	26.7	9.13	22.0	11.2	16.0
4254	12.3	20	4.36	9.46	4.86	8.90	4.17	20.2	3.74	4.38	9.80	15.0	12.4	6.27
4321	11.0	25	4.65	16.2	3.85	13.0	1.99	22.9	2.50	10.3	6.16	20.0	7.81	14.6
4579	11.4	18	5.43	12.9	2.76	8.75	1.08	18.4	1.52	14.7	4.68	15.5	6.16	10.7
4736	4.2	29	8.21	9.02	5.63	19.9	0.750	20.1	3.09	34.6	3.43	17.6	3.61	14.8
5055	10.0	32	4.46	11.8	3.67	6.04	1.64	30.2	2.54	8.97	5.34	25.0	5.91	16.3
5194	7.9	32	4.17	20.0	4.14	14.0	1.53	28.4	3.07	13.2	4.83	27.3	5.57	21.3
5457	9.0	39	6.83	12.5	4.53	16.0	1.51	37.3	2.84	13.5	5.85	27.8	7.08	19.2
6946	7.5	41	6.96	28.3	6.64	24.1	3.07	34.8	4.71	18.4	9.22	31.6	12.0	23.7
7331	9.0	20	6.55	10.1	4.69	5.56	1.46	23.0	3.10	10.2	5.55	13.8	6.83	5.88
$N_{\text{fit}}=16$		415		16.5		15.7		26.8		17.9		21.5		16.6
$N_{\text{fit}}=1$		415	6.68	21.7	4.85	17.9	1.60	32.4	3.05	20.9	5.94	24.6	7.30	22.3

^aUnits: $M_\odot \text{yr}^{-1} \text{kpc}^{-2}$

TABLE 3
RMS DISPERSION OF STAR FORMATION LAW RESIDUALS ($\log_{10} R_{\text{sfr}}$)^a

	$N_{\text{fit}} = 16$	$N_{\text{fit}} = 14$	$N_{\text{fit}} = 16$		$N_{\text{fit}} = 1$	
Star Formation Law	Molecular Dominated	Molecular Rich	Entire Regions	Molecular Dominated	Molecular Rich	Entire Regions
Kennicutt-Schmidt	0.165 (0.149)	0.0567	0.161 (0.144)	0.229 (0.217)	0.151	0.217 (0.204)
Constant Molecular	0.150 (0.131)	0.0672	0.153 (0.135)	0.181 (0.164)	0.161	0.179 (0.166)
KM05	0.254 (0.228)	0.0718	0.263 (0.237)	0.312 (0.285)	0.310	0.323 (0.301)
KMT09	0.164 (0.134)	0.0727	0.176 (0.142)	0.205 (0.184)	0.209	0.208 (0.192)
Gas- Ω	0.218 (0.191)	0.0563	0.211 (0.182)	0.248 (0.219)	0.215	0.246 (0.220)
GMC Collision	0.171 (0.146)	0.0559	0.163 (0.140)	0.223 (0.193)	0.219	0.222 (0.199)

^aResults in parentheses show the effect of excluding the $r < 1$ kpc regions

TABLE 4
STAR FORMATION LAW PARAMETERS FOR GALACTIC DYNAMICAL PROPERTY SUB-SAMPLES

		N_{ann}	A_g^{a} (10^{-2})	χ_g (10^{-2})	A_{H2}^{a} (10^{-2})	χ_{H2} (10^{-2})	A_{KM}^{a}	χ_{KM} (10^{-2})	$A_{\text{KMT}}^{\text{a}}$ (10^{-2})	χ_{KMT} (10^{-2})	B_{Ω} (10^{-3})	χ_{Ω} (10^{-2})	B_{CC} (10^{-3})	χ_{CC} (10^{-2})
Low $\bar{\beta}$	$N_{\text{fit}} = 9$	195		16.5		15.2		27.9		18.2		23.3		17.4
	$N_{\text{fit}} = 1$	195	7.34	24.4	4.91	17.8	1.21	31.6	0.03	20.7	5.16	25.9	6.19	21.4
High $\bar{\beta}$	$N_{\text{fit}} = 7$	138		17.5		15.6		23.3		14.6		20.9		17.6
	$N_{\text{fit}} = 1$	138	5.58	18.7	4.50	18.5	1.87	27.2	3.21	20.4	6.45	22.2	9.17	19.7
KS Test p			0.032		0.678		0.067		0.620		0.067		0.011	
Low \bar{v}	$N_{\text{fit}} = 7$	143		18.7		19.0		24.5		22.3		21.9		19.6
	$N_{\text{fit}} = 1$	143	7.39	23.1	5.65	20.0	1.83	31.2	3.86	23.9	6.84	25.1	9.22	24.6
High \bar{v}	$N_{\text{fit}} = 9$	190		15.5		11.9		27.2		10.9		22.7		15.8
	$N_{\text{fit}} = 1$	190	5.98	22.1	4.14	14.1	1.22	29.1	2.73	14.6	4.91	22.8	6.10	16.8
KS Test p			0.735		0.067		0.067		0.067		0.011		0.017	
Non-barred	$N_{\text{fit}} = 7$	134		15.6		12.0		27.1		12.6		22.9		16.2
	$N_{\text{fit}} = 1$	134	6.13	25.1	4.69	15.1	1.24	33.5	3.20	16.7	4.86	25.2	5.78	20.7
Barred	$N_{\text{fit}} = 9$	199		17.7		17.2		25.4		19.1		22.0		18.4
	$N_{\text{fit}} = 1$	199	6.85	21.2	4.77	20.0	1.61	28.7	3.15	22.8	6.27	23.6	8.50	20.9
KS Test p			0.620		0.996		0.358		0.790		0.155		0.017	

^aUnits: $M_{\odot}\text{yr}^{-1}\text{kpc}^{-2}$

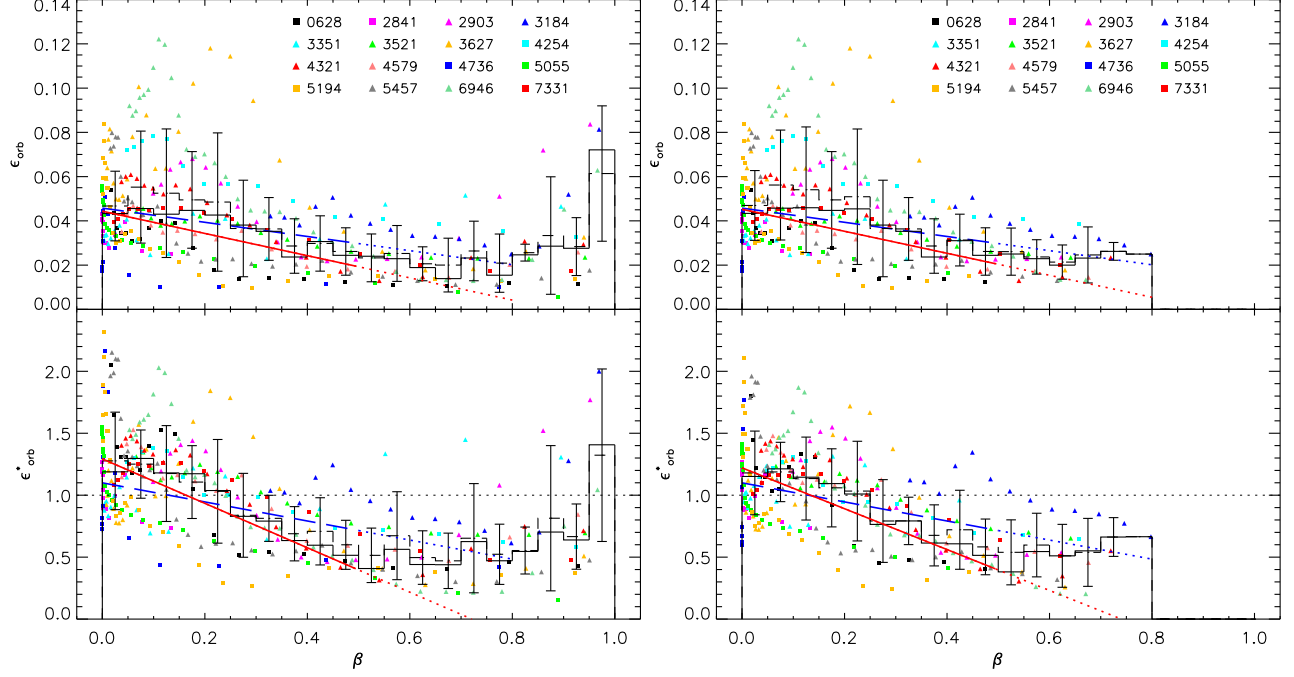


FIG. 5.— (a) Top left: Star formation efficiency per orbital time, ϵ_{orb} , as a function of rotation curve gradient, β . The data for the annuli in each galaxy are shown with different colors and symbols, as indicated. Also shown are the mean (black dashed) and median (black solid) of the data, together with 1σ dispersion, in uniform bins of β . The best fit linear relation $\epsilon_{\text{orb}} = \epsilon_{\text{orb},0}(1.0 - \alpha_{\text{cc}}\beta)$ for data in the range $0 < \beta < 0.5$ (see text for assumed errors) is shown by the solid red line (with extrapolation for $\beta > 0.5$ shown by a dotted line). The best fit linear relation with $\alpha_{\text{cc}} = 0.7$ from the GMC collision theory (for $\beta \ll 1$) is shown by the dashed blue line (with extrapolation for $\beta > 0.5$ shown again by a dotted line). (b) Bottom left: As above, but now showing normalized efficiency per orbit, $\epsilon_{\text{orb}}^* \equiv \epsilon_{\text{orb}} / \bar{\epsilon}_{\text{orb}}$ versus β . Each value has been normalized by the average for its particular galaxy. The best fit line for $\epsilon_{\text{orb}}^* = \epsilon_{\text{orb},0}^*(1.0 - \alpha_{\text{cc}}\beta)$ for data in the range $0 < \beta < 0.5$ is shown by the solid red line, and that for $\alpha_{\text{cc}} = 0.7$ by the dashed blue line (with extrapolations for $\beta > 0.5$ shown by dotted lines). (c) Top right: Same as (a), but now excluding all data at $r < 1$ kpc. (d) Bottom right: Same as (b), but now excluding all data at $r < 1$ kpc. In all panels, a trend of declining efficiency with increasing β (i.e. decreasing shear rate) is seen: there is about a factor of two decrease as β rises from 0 (flat rotation curve case) to 0.5.

general, none of the star formation laws show very significant probabilities for systematic differences between the Low and High β sub-samples, in part because of the small numbers in these samples.

The most significant of these is the approximately 1% probability that the B_{CC} 's from the GMC Collision model are drawn from the same distribution. This could be explained by the fact that because the equation for the star formation rate (eq. 6) depends on both B_{CC} and β , these quantities become (inversely) correlated: i.e., a galaxy with high β tends to need a larger value of B_{CC} to yield a given star formation rate. Given the relatively low significance of the probability, little more can be concluded for these trends with mean galactic shear until larger samples of galaxies are available.

We can, however, look in more detail at each galactic annulus and test for the prediction of the GMC Collision law that the star formation efficiency per orbit, $\epsilon_{\text{orb}} = (2\pi/\Omega)\Sigma_{\text{sfr}}/\Sigma_g$, should decline as the *local* value of β in a given annulus increases. In the Gas- Ω model, $\epsilon_{\text{orb}} = 2\pi B_{\Omega}$ is constant. In the GMC Collision model, $\epsilon_{\text{orb}} = 2\pi B_{\text{CC}}Q^{-1}(1 - 0.7\beta)$ (for $\beta \ll 1$). The star formation rate and efficiency decline with increasing β because a lower shear rate leads to a smaller rate of GMC collisions.

To test for this effect, in Figure 5 we show ϵ_{orb} versus β for each annulus (data from each galaxy are shown with different colors and symbols) together with the mean, median and 1σ dispersion in binned intervals of β . We also show a graph of $\epsilon_{\text{orb}}^* \equiv \epsilon_{\text{orb}} / \bar{\epsilon}_{\text{orb}}$, i.e., where each value has been normalized by the average for its particular galaxy. Versions of these graphs where all data at $r < 1$ kpc have been excluded are also shown.

A trend of declining efficiency with increasing β is seen: there is about a factor of two decrease as β rises from 0 (flat rotation curve case) to 0.5. There is a flattening and hint of an upturn in ϵ_{orb} and ϵ_{orb}^* as β reaches 1 (solid body rotation), but there are very few data points near $\beta = 1$ and, as can be seen from Figure 5c and d, those that exist are all located at galactic centers, where there may be larger systematic uncertainties, e.g., in determining the rotation curve shape (perhaps producing overestimated values of β in regions where the rotation curve is insufficiently resolved). On the other hand, the main trend of declining efficiency with increasing β is not driven by the presence of the very central regions: we further test for this by excluding data from the central 1, 2, 3 kpc and find essentially the same results for $\beta < 0.8$. This also indicates that the decline in ϵ_{orb}^* is not being driven by a systematic change in the “X-factor” that is needed to estimate Σ_{H_2} from observed CO line intensity, since Sandstrom et al. (2013) find this conversion factor is constant in these galaxies in all but the very inner ~ 1 kpc regions.

To gauge the decline of star formation efficiency per orbit with β more quantitatively and to assess the significance of this trend, for the data in the range $0 < \beta < 0.5$, we derive the best-fit function $\epsilon_{\text{orb}} = \epsilon_{\text{orb},0}(1 - \alpha_{\text{CC}}\beta)$, finding

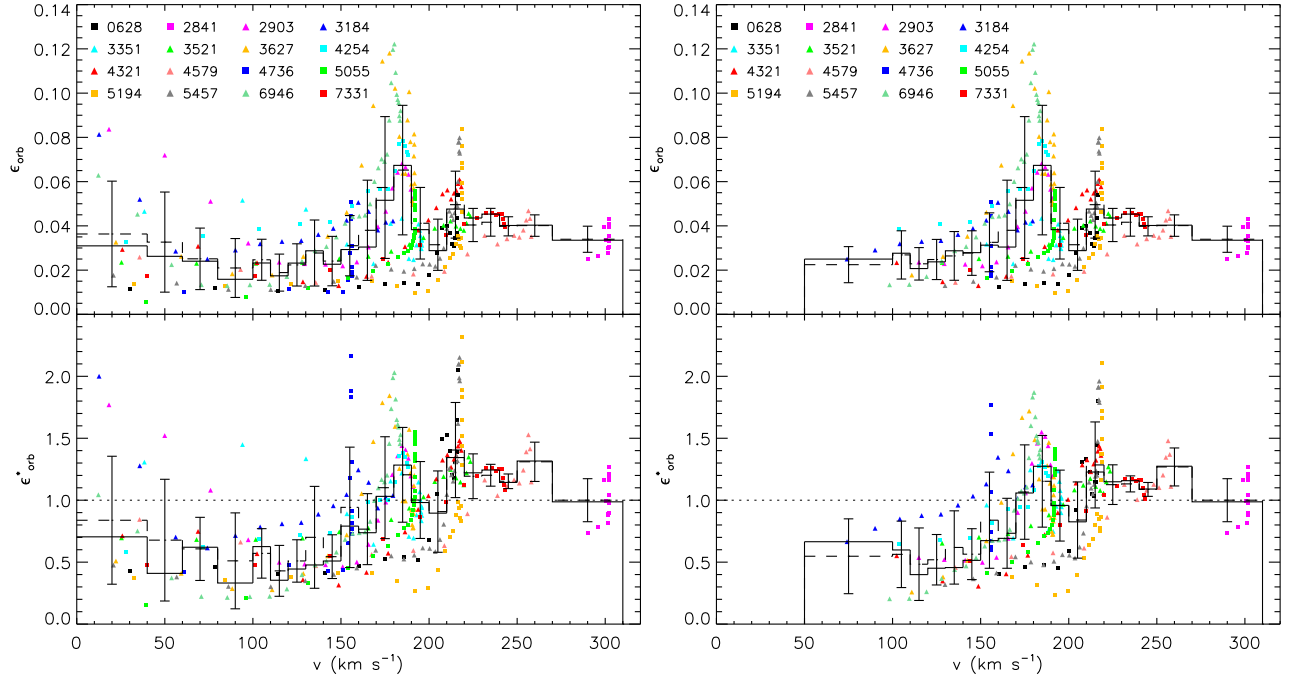


FIG. 6.— (a) Top left: Star formation efficiency per orbital time, ϵ_{orb} , as a function of rotation velocity, v . The data for the annuli in each galaxy are shown with different colors and symbols, as indicated. Also shown are the mean (dashed line) and median (solid line) of the data, together with 1σ dispersion, in uniform bins of v . (b) Bottom left: Normalized efficiency per orbit, $\epsilon_{\text{orb}}^* \equiv \epsilon_{\text{orb}}/\bar{\epsilon}_{\text{orb}}$ versus v . Each value has been normalized by the average for its particular galaxy. (c) Top right: Same as (a), but now excluding all data at $r < 1$ kpc. (d) Bottom right: Same as (b), but now excluding all data at $r < 1$ kpc. In all panels, a trend of increasing efficiency with increasing v up to $v \simeq 170$ km s $^{-1}$ is seen (see text).

$\epsilon_{\text{orb},0} = 0.044 \pm 0.005$ and $\alpha_{\text{CC}} = 1.13 \pm 0.49$ when using data that include the galactic centers and $\epsilon_{\text{orb},0} = 0.045 \pm 0.005$ and $\alpha_{\text{CC}} = 1.10 \pm 0.44$ when excluding data at $r < 1$ kpc (with the errors based on an assumption of 50% typical uncertainties in the absolute values of Σ_{sfr} and Σ_g and a 20% uncertainty in Ω , yielding 73% uncertainty in ϵ_{orb} to which we also add a minimum threshold uncertainty equal to the observed standard deviation of 0.022, and an assumed 30% plus threshold of 0.14 uncertainty in β). This best fit function is shown by the red solid line in Figure 5. Note, this line tends to sit below the binned mean and median values because the assumed errors in ϵ_{orb} have a component that is proportional to ϵ_{orb} .

Similarly for ϵ_{orb}^* we derive $\epsilon_{\text{orb},0}^* = 1.29 \pm 0.08$ and $\alpha_{\text{CC}}^* = 1.39 \pm 0.32$ when using data that include the galactic centers and $\epsilon_{\text{orb},0}^* = 1.22 \pm 0.08$ and $\alpha_{\text{CC}}^* = 1.35 \pm 0.31$ when excluding data at $r < 1$ kpc (with the errors based on an assumption of 25% typical uncertainties in the relative (disk-normalized) values of Σ_{sfr} and Σ_g and a 10% uncertainty in relative values of Ω , yielding 37% uncertainty in ϵ_{orb}^* to which we also add a minimum threshold uncertainty equal to the observed standard deviation of 0.40, and an assumed 30% plus threshold of 0.14 uncertainty in β). By this measure, a dependence of ϵ_{orb}^* on β (i.e., a non-zero value of α_{cc}) is detected at about the 4σ level, although the precise level of this significance is dependent on the rather uncertain assumptions about the size of the uncertainties.

Evaluating the Spearman rank correlation coefficient, r_s , and probability for chance correlation, p_s , for these data (i.e., for $0 < \beta < 0.5$), we find $r_s = -0.27$ and $p_s = 1.1 \times 10^{-5}$ for ϵ_{orb} versus β (essentially the same values are found if the $r < 1$ kpc data are excluded) and $r_s = -0.49$ and $p_s = 4.8 \times 10^{-17}$ for ϵ_{orb}^* versus β ($r_s = -0.44$ and $p_s = 1.6 \times 10^{-13}$ are found if the $r < 1$ kpc data are excluded), which suggests we may have been too conservative in our estimates of the uncertainties. Thus we conclude there is strong evidence of declining star formation efficiency per orbit with increasing rotation curve gradient β (i.e. declining shear).

Such a decline in star formation efficiency with increasing β , i.e., decreasing shear rate, is the opposite of what would be expected if formation of star-forming clouds (i.e., GMCs) from the diffuse interstellar medium via gravitational instability was the rate limiting step for galactic star formation rates, since increasing shear acts to stabilize gas disks. However, such a decline is predicted by the GMC Collision model (formally with $\alpha_{\text{CC}} \simeq 0.7$) for galactic star formation rates, where the rate limiting step for star formation is formation of star-forming clumps within GMCs via shear-driven GMC-GMC collisions (Tan 2000). Figure 5 also shows the predicted ϵ_{orb} and ϵ_{orb}^* versus β relation (i.e., based on eq. 6) from the GMC Collision model for the range $0 < \beta < 0.5$ (note, this model was developed for $\beta \ll 1$): it provides a reasonable match to the data, although with a somewhat shallower slope α_{CC} .

4.2.2. Rotation Speed

We divide the galaxy sample into “Low \bar{v} ” and “High \bar{v} ” sub-samples with $\bar{v} = 173$ km s $^{-1}$ being the dividing line. There are 7 Low \bar{v} galaxies and 9 High \bar{v} galaxies. We repeat the analysis of §4.1 for these two sub-samples and the results

are shown in Table 4.

We again carry out a two-sample Kolmogorov-Smirnov (KS) test to see if the distribution of derived star formation law parameters of the individual galaxies in each sub-sample are consistent with being drawn from the same parent distribution. The probabilities that they do come from the same distribution are shown in Table 4. As with the similar analysis for galactic disk shear, there are no especially significant differences between the sub-samples. Both “dynamical” star formation laws, i.e., Gas- Ω and GMC Collision that involve galactic rotation as an input, show potential differences in the sub-samples at the $1 - \sim 0.01$ probability. For this sample, Low \bar{v} galaxies show higher star formation efficiency per mean orbital time, similar to results reported by Leroy et al. (2013). However, such a trend is expected from simple correlated uncertainties, since, other things being equal, high velocity systems will tend to have shorter orbital times. So to explain a given star formation rate, a higher efficiency per orbit is needed.

We investigate the dependence of star formation efficiency per orbit with local v in a given annulus in Figure 6. A trend of increasing efficiency with increasing v is seen. This is consistent with the results of §4.2.1 showing declining efficiency with increasing β , since high β regions tend to have low v (being near galactic centers).

Note, this trend of increasing efficiency with increasing local v is the opposite of the trend with \bar{v} , discussed above. Such opposite behavior was also seen for the dependence of ϵ_{orb} on β and $\bar{\beta}$. This may indicate that the trends in galaxy averages, which are based on just 16 data points and which do not span a very wide dynamic range, are being driven by correlated uncertainties in ϵ_{orb} and $(\bar{\beta}, \bar{v})$. We expect that the more reliable indicator of the effect on star formation efficiency per orbit of these galactic properties is that shown by ϵ_{orb} and ϵ_{orb}^* versus local values of β and v , since they are based on a larger number of independent data points that span a wider dynamic range.

Figure 6 shows a relatively constant average value of $\epsilon_{\text{orb}} \simeq 0.04$ at velocities $\gtrsim 170 \text{ km s}^{-1}$. This indicates that these mostly flat rotation curve galactic star-forming disks can be treated as self-similar systems, turning a small, fixed fraction of their local total ($\text{H}_2 + \text{HI}$) gas content to stars every local orbit, as described in both the Gas- Ω and GMC Collision models.

4.2.3. Presence of a Bar

To test the effects on derived star formation law parameters of the presence of a bar we make the following division of the main galaxy sample. The non-barred sub-sample (with 7 galaxies) contains only normal spiral galaxies (SAa - Sac). The barred sub-sample (with 9 galaxies) contains both barred type galaxies (SBb) and transition type galaxies (SABb - SABbc).

As above, we carry out a two-sample Kolmogorov-Smirnov (KS) test to see if the distribution of derived star formation law parameters of the individual galaxies in each sub-sample are consistent with being drawn from the same parent distribution. The probabilities that they do come from the same distribution are shown in Table 4. Again, there are no especially significant differences between the sub-samples. The GMC Collision model shows a potential difference in the sub-samples at the $1 - \sim 0.01$ probability, with barred galaxies having a larger average value of B_{CC} (i.e. higher star formation efficiency per orbit) than non-barred galaxies by about 50%. In the context of this model, this might indicate an enhancement in GMC-GMC collision rates with the presence of a bar (which is likely also correlated with the presence of spiral arms in the main star-forming disk; orbit crowding in spiral arms may lead to enhanced GMC collision rates, e.g., Dobbs 2013), but a larger sample of galaxies is needed to be able to test the significance of this potential effect. We note on the other hand that Meidt et al. (2013) have claimed there is actually a suppression of star formation (longer molecular gas depletion times) in the spiral arms of M51 due to enhanced streaming motions.

On fitting the Gas- Ω law, a modestly higher (by a factor of about 1.3) star formation efficiency per orbit, $\epsilon_{\text{orb}} = 2\pi B_{\Omega}$, is also seen in the barred compared to non-barred galaxies. However, the KS probability of the samples having the same intrinsic distributions of efficiency parameters is a relatively large 0.16, i.e., the effect is not very significant. This result is consistent with that noted in the study of a larger sample of more distant, less well-resolved galaxies by Saintonge et al. (2012), who found a factor of 1.5 enhancement in molecular gas depletion rates ($\propto \Sigma_{\text{sfr}}/\Sigma_{\text{H}_2}$) in their barred sample compared to their control sample (but with an even larger KS probability of 0.25 of the samples being the same).

Finally we note that there are correlations amongst the properties of the sub-samples: e.g., most barred galaxies are also high β galaxies. Thus one needs to be careful in attributing primary cause of an effect on star formation to these dynamical properties.

5. DISCUSSION AND CONCLUSIONS

We have tested six star formation laws against the resolved profiles of 16 molecular dominated and molecular rich regions of nearby, massive disk galaxies. There is a range from about a factor of 1.4 to 1.8 dispersion in the residuals of the best-fits when allowing each galaxy one free parameter to normalize the star formation laws, rising to 1.5 to 2.1 when a single global parameter is fit to the sample for each law.

Since the different laws involve different inputs, which can have varying levels of observational uncertainties and varying degrees to which they connect to fundamental galactic physical properties, the relative ordering of the laws is not of primary importance (formally, the Constant Molecular law does best in having the smallest residuals; see Table 3).

More interesting is the comparison of laws within similar classes. Thus the turbulence-regulated model of KMT09 is seen to be a clear improvement over the KM05 model. The GMC Collision model improves over the Gas- Ω model.

The reason for this latter effect is the predicted decrease in star formation efficiency per orbital time with decreasing shear rate (increasing β) in the disk due to a reduced rate of shear-driven GMC-GMC collisions (Gammie et al. 1991;

Tan 2000; Tasker & Tan 2009), which is elucidated in Figure 5. We estimate that the significance of this trend over the range $0 < \beta < 0.5$ is at least at the 4σ level. Such a trend is the opposite of that expected if development of gravitational instabilities (e.g., leading to GMC formation) from the diffuse interstellar medium is the rate limiting step for star formation activity.

Confirmation of this result with a larger sample of galaxies, together with more careful investigation of potential systematic uncertainties, such as galactic radial gradients in normalization of star formation rate indicators and CO to H₂ conversion factors (although this latter does not appear to be a major effect; Sandstrom et al. 2013), is desirous.

More tentatively, we have found evidence that the presence of a bar boosts star formation efficiency per orbit. This could potentially be due to the influence of the bar on the strength of spiral arms (or more general axisymmetric structure; Kendall et al. 2011) in the larger-scale star-forming disks of the galaxies, although the influence of spiral arms on star formation activity in NGC 628, NGC 5194 and NGC 6946 has been found to be small ($\lesssim 10\%$) (Foyle et al. 2010). More detailed study of the influence of spiral arms (including potential inducement by the presence of bars) and their effect on star formation efficiency per orbit in a larger sample of galaxies is needed. Also worthwhile is further theoretical work on the influence of bars and spiral arms on the global GMC collision rate and its link to star formation, i.e., compared to that in more axisymmetric, flocculent galaxies.

CS acknowledges support from the Royal Thai Government Scholarship. JCT acknowledges NASA Astrophysics Theory and Fundamental Physics grant ATP09-0094. This research has made use of the NASA/IPAC Extragalactic Database (NED), which is operated by the Jet Propulsion Laboratory, California Institute of Technology, under contract with the National Aeronautics and Space Administration.

REFERENCES

- Bell, T. A., Viti, S. & Williams, D. A. 2007, MNRAS, 378, 983
 Bigiel, F., Leroy, A., Walter, F. et al. 2008, AJ, 136, 2846
 Blitz, L., Fukui, Y., Kawamura, A., Leroy, A., Mizuno, N., & Rosolowsky, E. 2007, in *Protostars & Planets V*, eds. B. Reipurth, D. Jewitt, & K. Keil, (U. Arizona: Tucson), p.81
 Daddi, E., Elbaz, D., Walter, F. et al. 2010, ApJ, 714, L118
 Dobbs, C. 2013, IAU S, 298 (arXiv:1307.7133)
 de Blok, W. J. G., Walter, F., Brinks, E. et al. 2008, AJ, 136, 2648
 Elmegreen, B. G. 1994, ApJ, 425, L73
 Elmegreen, B. G. 2002, ApJ, 577, 206
 Foyle, K., Rix, H.-W., Walter, F., & Leroy, A. 2010, ApJ, 725, 534
 Gammie, C. F., Ostriker, J. P., & Jog, C. J. 1991, ApJ, 378, 565
 García-Burillo, S., Usero, A., Alonso-Herrero, A. et al. 2012, A&A, 539, 8
 Genzel, R., Tacconi, L. J., Gracia-Carpio, J. et al. 2010, MNRAS, 407, 2091
 Israel, F. P. 2009, A&A, 493, 525
 Kendall, S., Kennicutt, R. C., & Clarke, C. 2011, MNRAS, 414, 538
 Kennicutt, R. C. 1989, ApJ, 344, 685
 Kennicutt, R. C. 1998, ApJ, 498, 541 (K1998)
 Kennicutt, R. C. & Evans, N. J. 2012, ARA&A, 50, 531
 Krumholz, M. R., & McKee, C. F. 2005, ApJ, 630, 250 (KM2005)
 Krumholz, M. R., McKee, C. F., & Tumlinson, J. 2009, ApJ, 699, 850 (KMT2009)
 Krumholz, M. R., Dekel, A., & McKee, C. F. 2012, ApJ, 745, 69
 Larson, R.B. 1988, in *Galactic and Extragalactic Star Formation*, ed. R.E. Pudritz & M. Fich, Dordrecht: Kluwer, 435
 Leroy, A. K., Walter, F., Brinks, E. et al. 2008, AJ, 136, 2782
 Leroy, A. K., Walter, F., Sandstrom, K., et al. 2013, AJ, 146, 19
 Li, Y., Mac Low, M.-M., & Klessen, R. S. 2006, ApJ, 639, 879
 Matzner, C. D. 2002, ApJ, 566, 302
 Meidt, S. E., Schinnerer, E., García-Burillo, S. et al. 2013, ApJ, 779, 45
 Ostriker, E. C., McKee, C. F., & Leroy, A. K. 2010, ApJ, 721, 975
 Saintonge, Á, Tacconi, L. J., Fabello, S. et al. (2012), ApJ, 758, 73
 Schrubba, A., Leroy, A. K., Walter, F. et al. (2011), AJ, 142, 37
 Solomon, P. M., Rivolo, A. R., Barrett, J., Yahil, A. 1987, ApJ, 319, 730
 Tan, J. C. 2000, ApJ, 536, 173 (T2000)
 Tan, J. C. 2010, ApJ, 710, 88 (Paper I)
 Tasker, E. J. & Tan, J. C. 2009, ApJ, 700, 358
 Toomre, A. 1964, ApJ, 139, 1217
 Sandstrom, K. M., Leroy, A. K., Walter, F. et al. (2013), ApJ, 777, 5
 Walter, F., Brinks, E., de Blok, W. J. G. et al. 2008, AJ, 136, 2563
 Wang, B., & Silk, J. 1994, ApJ, 427, 759